Entanglement entropy of disordered quantum chains following a global quench

Y. Zhao, F. Andraschko, and J. Sirker
Department of Physics and Astronomy, University of Manitoba, Winnipeg, Manitoba, Canada R3T 2N2
(Received 13 February 2016; published 25 May 2016)

We numerically investigate the growth of the entanglement entropy $S_{\rm ent}(t)$ in time t, after a global quench from a product state, in quantum chains with various kinds of disorder. The main focus is, in particular, on fermionic chains with bond disorder. In the noninteracting case at criticality we numerically test recent predictions by the real-space renormalization group for the entanglement growth in time, the maximal entanglement as a function of block size, and the decay of a density-wave order parameter. We show that multiprecision calculations are required to reach the scaling regime and perform such calculations for specific cases. For interacting models with binary bond disorder we present data based on infinite-size density matrix renormalization group calculations and exact diagonalizations. We obtain numerical evidence of a many-body localized phase in bond-disordered systems where $S_{\rm ent}(t) \sim \ln t$ seems to hold. Our results for bond disorder are contrasted with the well-studied case of potential disorder.

DOI: 10.1103/PhysRevB.93.205146

I. INTRODUCTION

A method commonly used to study nonequilibrium dynamics in cold atomic gases and trapped-ion systems is a global quench, a sudden change of a global control parameter [1–3]. Numerically, such dynamics can be studied by approximating the time-evolved quantum state by a matrix product state (MPS) [4–10]. The time interval accessible by this method is determined by the rate at which the entanglement grows because an MPS with a finite matrix dimension can only faithfully approximate weakly entangled states. It is therefore of great interest to understand precisely how the entanglement depends on time following a quantum quench. While this question has already been studied extensively for clean systems [11–13], disordered systems have only recently come into focus [14–17]. In such systems entanglement can also provide a novel viewpoint to study localization. This is particularly useful in interacting many-body systems where a picture based on single-particle states and related localization measures are not applicable.

In a generic clean quantum system we expect that the entanglement of most eigenstates follows a volume law. A well-known exception is the ground state of a local Hamiltonian which typically shows an area-law scaling [18]. Given that a generic initial state in a quantum quench is a linear combination of many different eigenstates of the Hamiltonian responsible for the unitary time evolution, the entanglement of an infinite system, in general, grows without bounds as a function of time. A commonly used measure of entanglement for many-body systems is the entanglement entropy

$$S_{\rm ent}(t) = -\,\mathrm{Tr}\,\rho_A(t)\ln\rho_A(t), \tag{1}$$

which is the von Neumann entropy of a reduced density matrix $\rho_A(t) = \mathrm{Tr}_B\,\rho(t)$ obtained from the regular density matrix $\rho(t)$ by splitting the system into two parts, A and B, and taking a partial trace.

The entanglement growth $S_{\rm ent}(t)$ is best understood for a global quench in a one-dimensional conformally invariant system [12,19]. In this case, conformal field theory predicts a linear increase of the entanglement in time for $vt < \ell$, where v is the velocity of excitations and ℓ is the length of block A. For $vt > \ell$ the entanglement entropy saturates. This behavior can physically be understood in a picture of entangled quasiparticles which move in opposite directions [19]. The light-cone-like spreading implied by this picture is consistent with the Lieb-Robinson bounds [20,21].

Conformal field theory works surprisingly well even on a quantitative level for quenches in one-dimensional critical lattice models where conformal invariance only holds approximately at low energies. Consider, for example, the free spinless fermion model (XX model) with Hamiltonian

$$H = -\sum_i J_i(c_i^\dagger c_{i+1} + \mathrm{H.c.}) - \sum_i \mu_i(c_i^\dagger c_i - 1/2) \tag{2}$$

in the clean case $J_i = J \equiv 1$ and with $\mu_i = 0$. Here $c_i^{(\dagger)}$ annihilates (creates) a spinless fermion at site i. As the initial state for the quantum quench we consider in the following (unless stated otherwise) the density-wave product state

$$|D\rangle = \prod_i c_{2i}^\dagger |0\rangle, \tag{3}$$

where $|0\rangle$ denotes the vacuum. At low energies, the spectrum can be linearized around the two Fermi points, and the model becomes conformally invariant in this approximation.

For a free-fermion model such as the XX model in Eq. (2) the eigenvalues of the reduced density matrix $\rho_A(t)$ can be obtained by an exact diagonalization (ED) of the matrix of two-point correlations in the time-evolved state $|D(t)\rangle = e^{-iHt}|D\rangle$ (see Refs. [22–24] for details). In Fig. 1, results for $S_{\rm ent}(t)$ obtained numerically for model (2) and various system sizes N are shown. Here we have used open boundary conditions (OBC), and the block size is fixed to $\ell = N/2$.

In this case, conformal field theory predicts that

$$S_{\rm ent} \sim \begin{cases} \frac{\pi c t}{12\tau_0} & vt < \ell, \\ \frac{\pi c \ell}{24\tau_0} & vt > \ell, \end{cases} \tag{4}$$

where $v = 2$ with central charge $c = 1$ [19]. We therefore expect a crossover at times $t^* = \ell/v = N/4$ from a linear increase to saturation. This behavior is nicely confirmed by the data shown in Fig. 1(a). Note also that while the scale τ_0 in Eq. (4) is nonuniversal, the ratio of the slope of the linear

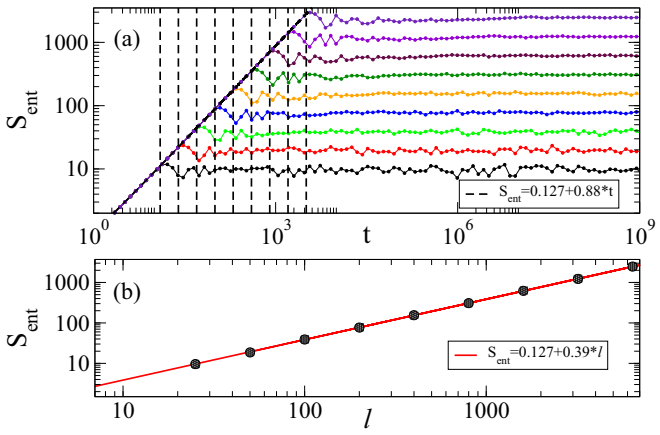

FIG. 1. (a) $S_{\rm ent}(t)$ for the open XX chain without disorder. Symbols denote ED data for system sizes $N = 50,100,200,400,800,1600,3200,6400,12\,800$ (from bottom to top); solid lines are a guide to the eye. The dashed vertical lines denote the crossover scale $t^* = \ell/2$. (b) Symbols show the saturation value as a function of block size ℓ. The fits in (a) and (b) show that $S_{\rm ent} \sim at$ for $t < t^*$ and a saturation at $S_{\rm ent} \sim \frac{a}{2}\ell$ for $t > t^*$.

increase at times $t < t^*$ and the saturation value at $t > t^*$ is universal because τ_0 cancels out. This quantitative prediction is also approximately fulfilled for the considered lattice model, as can be seen from the fits in Figs. 1(a) and 1(b).

Recently, there has been renewed interest in localization phenomena in *interacting* many-body systems [25–27]. In one-dimensional Heisenberg models with potential disorder it has been argued, based on exact diagonalization data, that there is a transition at finite disorder strength between an ergodic and a many-body localized (MBL) phase [28]. One of the main features used to identify an MBL phase after a quantum quench is the slow logarithmic growth of the entanglement entropy [16]. This has to be contrasted with the linear growth in the clean case and a saturation, $\lim_{t\to\infty}\lim_{\ell\to\infty}\lim_{N\to\infty} S_{\rm ent}(N,\ell,t) =$ const, which might naively be expected in an Anderson insulating phase of noninteracting particles due to the finite localization length.

While disorder is always a relevant perturbation for a noninteracting one-dimensional quantum system [29], critical points or lines between localized phases can still exist, and the above picture for the entanglement growth in an Anderson insulator is, in general, too naive. Two well-known examples where critical behavior in a disordered system occurs are the transverse Ising chain and the XX model with bond disorder [30–34]. A real-space renormalization-group (RSRG) treatment, where the strongest bonds are successively eliminated, predicts that such systems are driven to an infinite-randomness fixed point where the *mean localization length* scales as

$$\xi_{\rm loc}(\varepsilon) \sim |\ln(\varepsilon)|^{\Psi}, \tag{5}$$

with a critical exponent Ψ, and is much larger than the *typical localization length* [34]. These systems therefore show a delocalization transition as a function of eigenenergy ε. For the ground-state entanglement entropy of a block of length ℓ in an infinite critical random system this implies $S_{\rm ent} \sim \ln \ell$ [35]. For the XX model with bond disorder the latter prediction has been confirmed by an extensive numerical study [36].

Lately, the RSRG treatment of critical disordered systems has been generalized to excited states by also allowing for projections of a bond onto higher-energy states [37–39]. This so-called RSRG-X approach allows, in particular, us to make predictions with regard to the time evolution of the entanglement following a quantum quench from a product state in noninteracting critical random systems. Since RSRG-X essentially yields the same infinite randomness structure for excited states as for the ground state, a logarithmic scaling with block size ℓ

$$\lim_{t\to\infty}\lim_{N\to\infty} S_{\rm ent} \sim b \ln \ell \tag{6}$$

of the saturation value is expected, mimicking the ground-state behavior. In the infinite system at large finite times we therefore expect $S_{\rm ent} \sim \ln L(t)$, where $L(t) \leqslant \ell$ is a length scale which, according to Eq. (5), is expected to scale as $L(t) \sim |\ln t|^{\Psi}$. This implies

$$\lim_{\ell\to\infty}\lim_{N\to\infty} S_{\rm ent} \sim a \ln(\ln t) \tag{7}$$

in the infinite system at long times. Furthermore, the ratio of the prefactors is given by $a/b = \Psi$ with the critical exponent Ψ defined in Eq. (5). Numerically, a $\ln(\ln t)$ scaling in a certain time interval has been observed for the critical random transverse Ising model [15]. Another specific prediction of the RSRG concerns a quench in the XX model from an initial state with density-wave order, Eq. (3). In this case, the density-wave order parameter is expected to decay as $\Delta n \sim 1/\ln^2 t$ at long times [38]. The latter result is expected to hold also in interacting models which are in a critical MBL phase. Equation (7), however, is expected to change to $S_{\rm ent} \sim (\ln t)^{\alpha}$ with $\alpha \geqslant 1$ in the presence of interactions. Furthermore, the saturation value, Eq. (6), will then follow a volume law, $S_{\rm ent} \sim \ell$, but will remain smaller than in a system where the subsystem A reaches thermal equilibrium.

In this paper we will present a thorough numerical analysis of the entanglement dynamics in generic and critical one-dimensional systems which can be described in terms of free fermions. In particular, we will test the various scaling predictions above, which have been obtained based on the RSRG-X approach. Our work extends and generalizes previous numerical studies of the entanglement dynamics in such systems [15,40] by considering both XX and transverse field Ising models with various types of disorder and by providing numerical data for larger systems and larger sample sizes and including multiprecision data required to access long times. For the interacting XXZ model we will try to bridge the gap between RSRG-X predictions for bond-disorder quenching from the Néel state and numerical studies which have so far concentrated mostly on potential disorder. Checking the RSRG-X predictions for the bond-disordered case numerically is important because the RSRG-X results for critical MBL phases are not applicable to the case of potential disorder.

Our paper is organized as follows: As an example for a generic disordered system of noninteracting particles we study $S_{\rm ent}(t)$ for the XX model, Eq. (2), with potential disorder in Sec. II. In Sec. III we present results for the critical XX model with bond disorder. In both sections we consider a box as

well as a binary disorder distribution. In Sec. IV we show that results qualitatively similar to those for the critical XX model with bond disorder are also obtained for the critical random transverse Ising model. Using exact diagonalizations of small systems and density-matrix renormalization-group (DMRG) calculations for infinite systems with binary bond disorder, we then investigate in Sec. V the entanglement growth once interactions are included. In Sec. VI we summarize our main results and discuss them in the light of the RSRG-X predictions and recent numerical studies of MBL phases.

II. GENERIC DISORDERED CHAINS OF NONINTERACTING FERMIONS

As an example for a generic, noncritical disordered system we consider in the following the XX chain, Eq. (2), with potential disorder μ_i drawn either from a box or a binary distribution and $J_i \equiv J = 1$ fixed.

Without disorder, there are three length scales in the problem: the chain length N, the dynamical scale vt, and the block length ℓ. For most of the paper we keep the block length fixed, $\ell = N/2$, reducing the number of independent length scales to 2. In the clean case there are therefore only two regimes with different scaling (see Fig. 1). With disorder, on the other hand, we have instead three independent length scales: $L_{\rm ent}(t)$, $\ell = N/2$, and $\xi_{\rm loc}$. Here $L_{\rm ent}(t)$ denotes the length scale over which particles are entangled, and $\xi_{\rm loc}$ is the localization length, which, in general, will depend on energy $\xi_{\rm loc} = \xi_{\rm loc}(\varepsilon)$. The simplest case is $\xi_{\rm loc} \gg \ell \gg 1$, corresponding to weak disorder, in which case the new length scale $\xi_{\rm loc}$ is completely irrelevant for the dynamics and we expect $L_{\rm ent}(t) \sim vt$, so that the results for the case without disorder approximately hold. The entanglement properties are expected to change once $\ell \sim \xi_{\rm loc}$. It is this regime which we want to analyze in detail in the following.

A. Box distribution

First, we consider box potential disorder $\mu_i \in [-W/2, W/2]$. We average over at least 2000 samples and make sure that the data are converged by comparing results for which a different number of samples have been used.

For very weak disorder, $W = 0.1$, and chain lengths up to $N = 1600$, we are in a regime with $\xi_{\rm loc} \gg \ell$, where the entanglement growth is indeed very similar to the case without disorder (see Fig. 2).

Only for the largest length shown, $N = 3200$, do deviations from a linear increase and a crossover at $t^* = N/4$ become clearly visible. For the localization length this means that $\xi_{\rm loc} \gtrsim 3200$. The increase of the entanglement entropy in time and the saturation value as a function of block length ℓ are still approximately linear for lengths $N < 3200$ (see the inset of Fig. 2). Note, however, that already for small system sizes the fluctuations in the saturation value are noticeably suppressed compared to the clean case.

Next, we consider the case $W = 1.0$, where we are able to investigate both regimes, $\xi_{\rm loc} > \ell$ and $\xi_{\rm loc} < \ell$. The results of exact diagonalizations are shown in Fig. 3.

The initial increase of $S_{\rm ent}$ roughly follows a power law with an exponent smaller than 1. For $N \lesssim 200$ the crossover

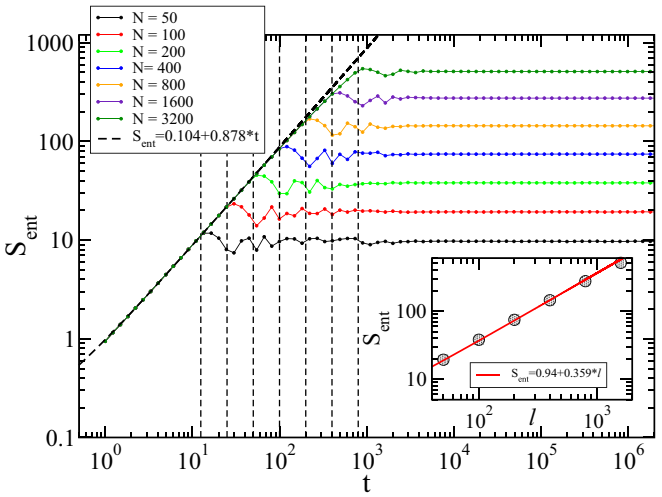

FIG. 2. $S_{\rm ent}$ for the open XX chain with box potential disorder $W = 0.1$. The dashed black lines denote the crossover scale $t^* = \ell/2$ in the clean case. Inset: Saturation value $S_{\rm ent}(\ell)$ for $t \to \infty$. The fits show that $S_{\rm ent} \sim at$ for $t < t^*$ and $S_{\rm ent} \sim \frac{a}{2}\ell$ for $t > t^*$ still approximately hold if $N < 3200$.

scale $t^* = \ell/2$ is still relevant and marks a deviation from the entanglement curve in the limit $\ell = N/2 \to \infty$. This means that for $N \lesssim 200$ a significant contribution from disorder configurations exists where quasiparticles can still be defined, propagate almost ballistically, and reach the end of the block at time t^*. For $N = 800$ and $N = 1600$ we have reached the regime where $\xi_{\rm loc} < \ell$ and the results are becoming independent of block size ℓ. The inset shows that the saturation values can be fitted by a simple exponential form. The length in the exponential fit should be interpreted as being roughly the localization length, $\xi_{\rm loc} \approx 100$. This picture is confirmed by a calculation of the stationary probability distribution $|\Psi(x, t \to \infty)|^2$ of a single particle which is located at the

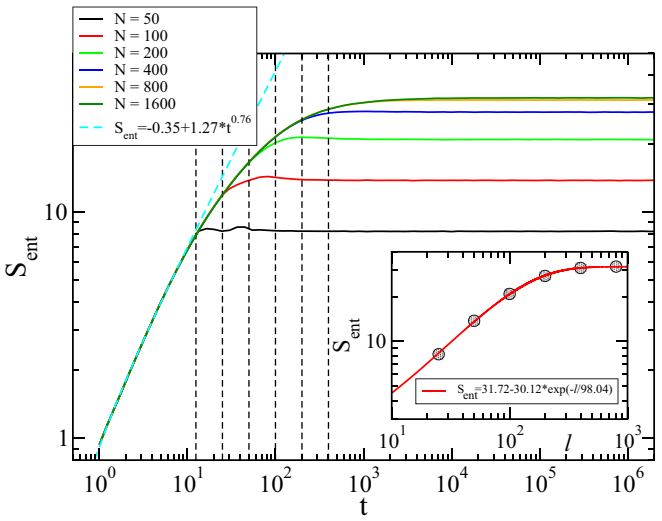

FIG. 3. $S_{\rm ent}$ for the open XX chain with box potential disorder $W = 1.0$. The dashed vertical lines denote the crossover scale $t^* = \ell/2$ in the clean system. Inset: Saturation value versus block length $\ell = N/2$.

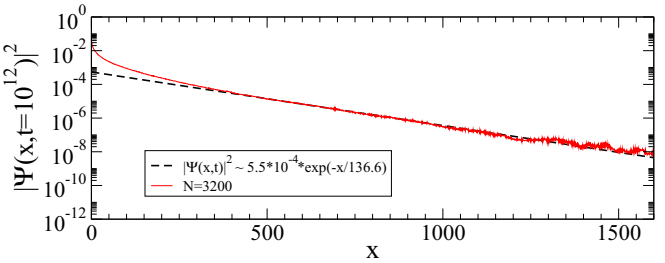

FIG. 4. Disorder averaged stationary probability distribution $|\Psi(x,t\to\infty)|^2$ for a single particle initially located in the middle of a chain ($x = 0$) with $N = 3200$ sites and disorder $W = 1.0$.

center of the chain at time $t = 0$. At long distances the decay is exponential, $|\Psi(x,t\to\infty)|^2 \sim \exp(-x/\xi_{\rm loc})$, with a fit yielding $\xi_{\rm loc} \sim 136$ (see Fig. 4).

The saturation value of the entanglement entropy as a function of block length ℓ thus allows us to obtain an estimate for the localization length $\xi_{\rm loc}$. Here we expect that the localization length only weakly depends on energy, so that typical and mean correlation lengths are of similar magnitude.

That the XX model with potential disorder is indeed a generic disordered system where a delocalization transition as a function of energy does not occur is supported further by an analysis of the spectral properties of the system. We define the density of states (DOS) as

$$\rho(\varepsilon) = \frac{\Delta N}{N\Delta\varepsilon}, \tag{8}$$

where $\Delta\varepsilon$ is the size of an energy bin and ΔN is the number of single-particle states in this bin. The DOS for $W = 1$ is shown in Fig. 5(a) and is peaked near the edges of the single-particle spectrum. For $W = 10$ the DOS becomes almost box shaped. To analyze how localized a particular single-particle eigenstate is we define a localization measure

$$I_\varepsilon = \sum_{l=-m}^{m} |\phi_\varepsilon(x_0+l)|^2, \tag{9}$$

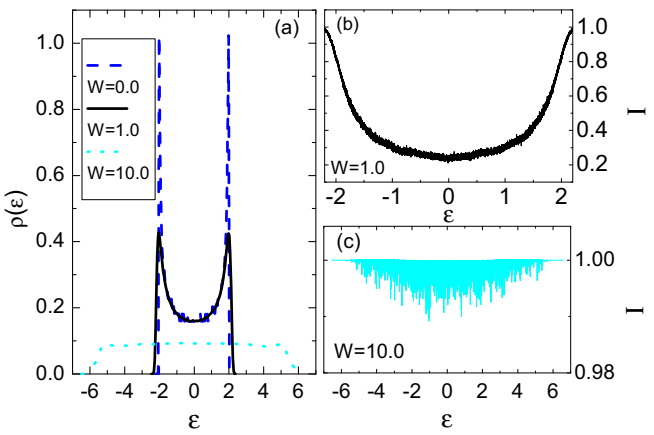

FIG. 5. XX model with potential disorder W and $N = 1000$ using 2000 samples: (a) DOS for $W = 0.0$, 1.0, and $W = 10.0$ using a bin size $\Delta\varepsilon = |\varepsilon_{\rm max}|/100$. (b) and (c) Localization measure I_ε, Eq. (9), with $m = 10$.

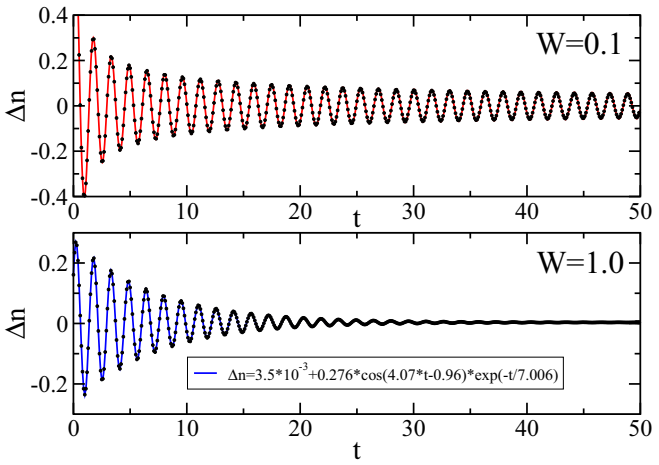

FIG. 6. Density-wave order parameter $\Delta n(t)$. The circles denote the numerical data. For weak disorder $W = 0.1$ the result closely resembles the clean case (solid line). For $W = 1.0$ the data are well fitted by an exponential decay to a finite value, Eq. (12) (solid line).

where ϕ_ε is the single-particle eigenfunction with eigenenergy ε and $\max_{x\in[1,N]} |\phi_\varepsilon(x)|^2 = |\phi_\varepsilon(x_0)|^2$. That is, I_ε measures how probable it is that the particle in eigenstate ϕ_ε is located in an interval $[x_0 - m, x_0 + m]$ around the position of the maximum in the probability distribution. Note that Eq. (9) is not the inverse participation ratio. We find that the latter does not always give a clear picture, in particular, for the critical systems studied later.

If we keep m fixed and send $N \to \infty$, then $I_\varepsilon \to 0$ if the state is delocalized. For $W = 1, 10$ and $m = 10$ we find that I_ε is converged for system size $N = 1000$ and nonzero for all energies [see Figs. 5(b) and 5(c)]. This confirms that all eigenstates are indeed localized.

Of experimental interest is the time evolution of the density-wave order parameter

$$\Delta n(t) = \frac{2}{N}\sum_j (-1)^j \langle n_j\rangle(t), \tag{10}$$

starting from the density-wave initial state, Eq. (3). For cold atomic gases $\Delta n(t)$ can be measured directly [41–43]. In the clean case we obtain, after taking the thermodynamic limit,

$$\Delta n(t) = J_0(4t) \sim (2\pi t)^{-1/2}\cos(4t - \pi/4), \tag{11}$$

where J_0 is the Bessel function of the first kind and we have used the asymptotic expansion at long times. For weak disorder $W = 0.1$ and short times, the order parameter closely follows the time evolution in the clean case (see Fig. 6). The decay in the time interval shown is therefore well described by a power law $\Delta n \sim 1/\sqrt{t}$ with deviations being expected at longer times.

In contrast, we find an exponential decay

$$\Delta n(t) = \Delta n_0 + a\cos(\Omega t - \phi)\exp(-t/\tau) \tag{12}$$

to a finite value $\Delta n_0 \approx 4\times 10^{-3}$ for disorder strength $W = 1.0$. Thus disorder prevents a full dephasing of Δn, and the nonzero value Δn_0 in the long-time limit is a signature of localization.

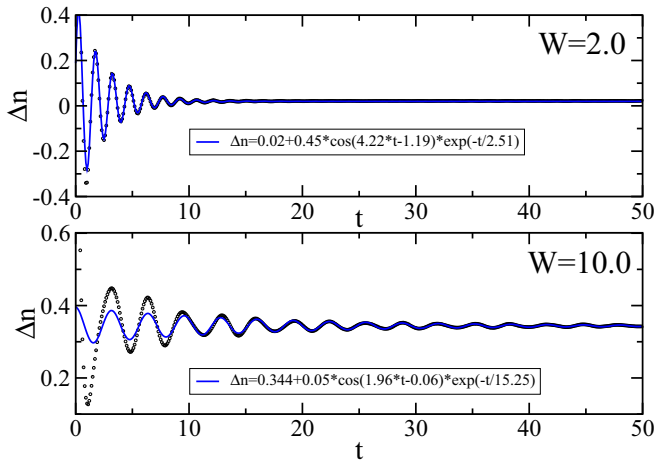

FIG. 7. Density-wave order parameter $\Delta n(t)$. The decay for $W = 2.0$ and $W = 10.0$ is still exponential; however, the decay rate τ is a nonmonotonic function of disorder. Lines are fits of the asymptotic behavior using Eq. (12).

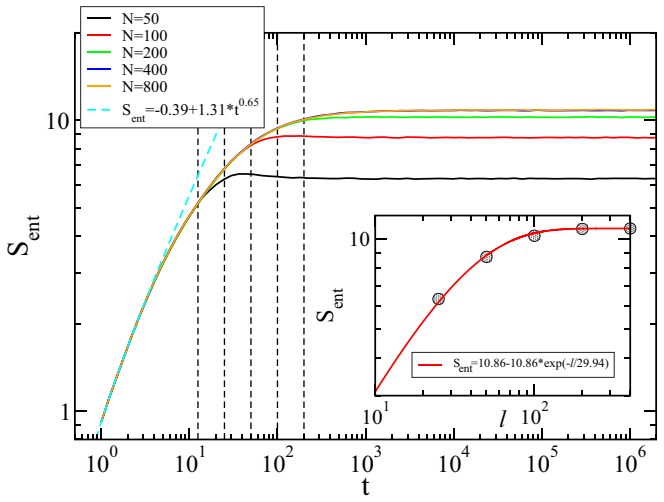

FIG. 8. $S_{\rm ent}$ for the open XX chain with binary potential disorder $W = 1.0$. The dashed vertical lines denote the crossover scale $t^* = \ell/2$ in the clean system. Note that the curves for $N = 400$ and $N = 800$ are almost on top of each other.

Note, however, that while the long-time mean Δn_0 is a monotonic function of disorder W, the decay time τ is not. This is obvious from the data shown in Fig. 7 which show very slowly decaying oscillations for $W = 10$. This behavior can be explained as follows: If $W \gg J$, then, for any disorder configuration, neighboring sites in the chain exist where the potential difference $|\mu_i - \mu_{i+1}|$ is much larger than the hopping J. Between these sites the chain is effectively cut, and the finite segments show almost independent dynamics. The case $W \to \infty$ can be analyzed analytically for a binary disorder distribution and is discussed in the next section.

B. Binary distribution

Systems with binary potential disorder $\mu_i = \pm W/2$ are ideal for numerical studies because an exact disorder average in the thermodynamic limit is possible even in the interacting case. The idea is to map the system with discrete disorder onto a translationally invariant system in an enlarged Hilbert space with ancilla sites, $\mu_i n_i \to \frac{W}{2} n_i \sigma_i$, where $\sigma_i = \pm 1$. Preparing the ancilla variables σ_i in a completely mixed state, a tracing over the ancillae then gives the exact disorder average of any local observable [17,44]. It is thus interesting to see if the binary disorder distribution gives qualitatively the same physics as the box disorder distribution considered previously.

A disadvantage of mapping the system with binary disorder onto a translationally invariant system with additional ancilla sites is that the only entanglement entropy one can then easily calculate is the entanglement entropy in the enlarged Hilbert space consisting of the real system *and* the ancillae [17]. This entanglement entropy will qualitatively show the same time dependence as $S_{\rm ent}$ of the system alone because the ancilla sites are static. A quantitative comparison with the box potential disorder, however, becomes impossible. In the following, we will therefore not map the system. Instead, we average over a set of samples as for the box distribution. We will, however, use the mapping onto a system with ancillae in Sec. V when we discuss interacting models with binary disorder.

Results for binary potential disorder $W = 1$ are shown in Fig. 8 and are qualitatively very similar to those for the box disorder case.

We find an increase at small times described approximately by a power law and a saturation at long times. The approach to saturation in the limit of infinite block size is again controlled by the localization length with $\xi_{\rm loc} \approx 30$ in the case considered here.

Let us finally discuss the case of infinite binary disorder, $W \to \infty$, following Ref. [17]. In this case the chain is cut into finite segments of equal potential. The probability of finding a segment of length l with constant potential is given by $p(l) = l/2^{l+1}$. For a quench starting from the initial state (3), the time evolution of the density-wave order parameter (10) can now be calculated straightforwardly,

$$\Delta n(t) = \sum_{l=1}^{\infty} p_l \Delta n_l(t). \tag{13}$$

Here $\Delta n_l(t)$ is the time evolution of a segment of length l with OBC and equal potential on all sites,

$$\Delta n_l(t) = \frac{2}{l} \sum_{k=1}^{l} \exp\left[4it \cos\left(\frac{\pi k}{l+1}\right)\right]. \tag{14}$$

The oscillations around the mean value $\overline{\Delta n}$, determined by the segments with odd length, $\overline{\Delta n} = \sum_l p_l \overline{\Delta n_l} = \sum_{l\ \rm odd} \frac{2}{l} p_l = \frac{1}{3}$, will therefore persist for all times (see Fig. 9).

III. XX MODEL WITH BOND DISORDER

Properties of the XX model, Eq. (2), with bond disorder $P(J)$, where P is an arbitrary distribution function of bonds J_i, and $\mu_i \equiv 0$ were studied first by Eggarter and Riedinger [30]. They found that the density of states $\rho(\varepsilon)$ shows a divergence at zero energy,

$$\rho(\varepsilon) \sim 1/|\varepsilon(\ln \varepsilon^2)^3|. \tag{15}$$

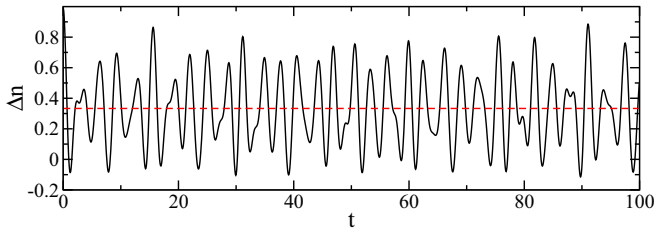

FIG. 9. Density-wave order parameter $\Delta n(t)$ for infinite binary disorder. The dashed line denotes the long-time mean $\overline{\Delta n} = 1/3$.

This behavior is confirmed numerically [see Fig. 10(a)].

The divergent density of states at $\varepsilon = 0$ is a consequence of particle-hole symmetry. The localization measure I_ε, Eq. (9), shown in Fig. 10(b) furthermore indicates that the system undergoes a delocalization transition at $\varepsilon \to 0$. The XX model with bond disorder is therefore an example of a critical disordered system.

More specifically, it has been shown that the *typical* localization length diverges [30],

$$\tilde{\xi}_{\rm loc} \sim |\ln \varepsilon^2|, \tag{16}$$

for $\varepsilon \to 0$. Later, it was emphasized that the spatial decay of the average Green's function is dominated by the mean localization length

$$\xi_{\rm loc} \sim |\ln \varepsilon^2|^2, \tag{17}$$

which is much longer than the typical localization length, Eq. (16) [31,34].

In recent years, a RSRG-X approach has also been used to investigate the quench dynamics in the XXZ chain with bond disorder leading to the following three specific predictions for the XX case [38]: (i) The asymptotic growth of entanglement entropy is given by

$$S_{\rm ent}(t) \approx \frac{S_p}{3} \ln[\ln(\Omega_0 t) + 1/a_0], \tag{18}$$

with $S_p = 2 - 1/\ln 2 \approx 0.557$. (ii) The entanglement entropy of a block of length ℓ in the thermodynamic limit saturates at

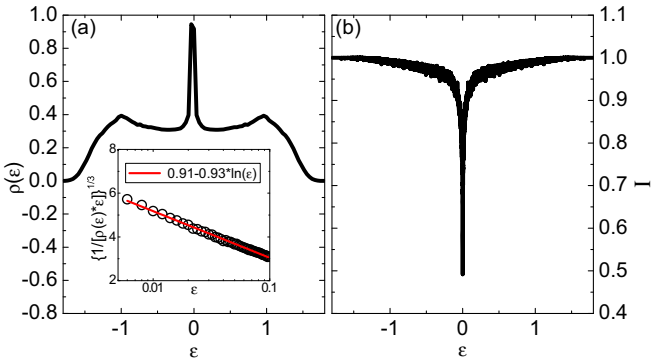

FIG. 10. Open XX chain with $N = 1000$ sites and bond disorder $J_i \in (0,1)$ using 1000 samples. (a) DOS based on 100 energy bins. Inset: Scaling $[|\varepsilon|\rho(\varepsilon)]^{-1/3} \sim |\ln \varepsilon^2|$ [see Eq. (15)] near $|\varepsilon| \sim 0$ using 1800 bins. (b) I_ε with $m = 10$: delocalization of eigenstates, $I_\varepsilon \to 0$ for $\varepsilon \to 0$ in the thermodynamic limit.

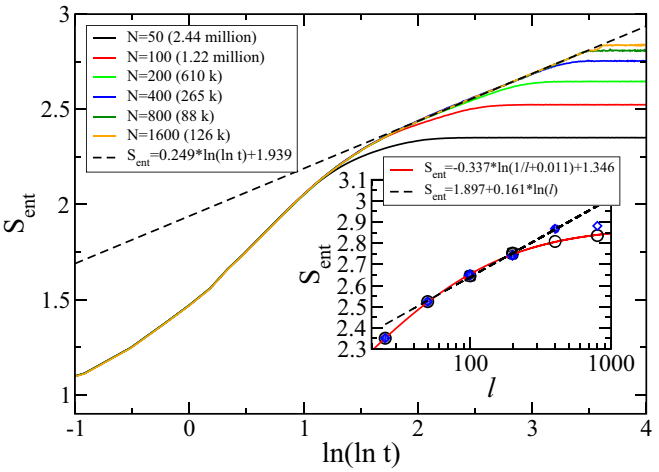

FIG. 11. $S_{\rm ent}(t)$ for the XX model with bond disorder $J_i \in (0,1)$ and PBC, obtained using standard double-precision arithmetics. The numbers in parentheses in the legend refer to the number of samples. The dashed line is a fit. Inset: Saturation value as a function of block length $\ell = N/2$ with circles denoting results in double precision and diamonds denoting results in double-double precision.

long times,

$$S_{\rm ent}(t \to \infty) \approx \frac{S_p}{6} \ln \ell. \tag{19}$$

(iii) For a quench starting from the density-wave state, Eq. (3), the order parameter (10) decays as

$$\Delta n(t) \approx [a_0 \ln(\Omega_0 t) + 1]^{-2}. \tag{20}$$

Here a_0 and Ω_0 are nonuniversal constants. In the following, we will test these scaling predictions using ED data, which will also allow us to analyze the regime of short and intermediate times where the RSRG-X approach is not applicable.

A. Box distribution

We start by considering chains of length N with periodic boundary conditions (PBC) and a box distribution $J_i \in (0,1)$. We keep the block size $\ell = N/2$ fixed. Data for $S_{\rm ent}(t)$, starting from the initial density-wave ordered state (3), are shown in Fig. 11.

A very well defined $\ln(\ln t)$ scaling is observed over several orders in time, consistent with the RSRG prediction, Eq. (18); however, the prefactor deviates from $S_p/3 \approx 0.186$. A problem for the numerical calculations is the long times required to observe saturation. In usual double precision, only 15 relevant digits are kept. The spectrum of the XX model with bond disorder contains, however, many very small eigenvalues ε_i (see Fig. 10). These eigenvalues and the corresponding eigenstates become relevant for the time evolution if $t\varepsilon_i \gtrsim 1$. Since eigenvalues smaller than 10^{-14} and their corresponding eigenvectors in a spectrum which also contains eigenvalues of order 1 cannot be determined accurately in double precision, we expect the numerical data in Fig. 11 to become unreliable for $\ln(\ln t) \gtrsim 3.5$. An indication of these numerical problems is a small dip in the curve for $N = 1600$ close to the times where the entanglement entropy starts to saturate.

The saturation value $S_{\rm ent}(\ell = N/2, t \to \infty)$ is shown in the inset of Fig. 11 on a logarithmic scale. A naive fit of the double-precision data seems to point to a saturation, $\lim_{\ell\to\infty} S_{\rm ent}(\ell = N/2, t \to \infty) \approx 2.9$. However, there are two problems with such a fit: (i) For $N = 50$ the regime where $S_{\rm ent}(t) \sim \ln\ln t$ is never reached. The related scaling of the saturation value $S_{\rm ent}(\ell, t \to \infty) \sim \ln \ell$ therefore cannot be expected to hold. System sizes $N \gtrsim 100$ are required. (ii) Only systems with $N \leqslant 400$ show a saturation at times $t \leqslant 10^{14}$. The saturation values for $N = 800$, 1600 obtained in double precision are not reliable. In order to overcome problem (ii) we have therefore also performed calculations in double-double precision where 30 relevant digits are kept and results for $t \lesssim 10^{30}$, corresponding to $\ln\ln t \lesssim 4.2$, are expected to be reliable. Here we have used the linear algebra package MPACK, which makes calculations in fixed double-double or quadruple precision as well as in arbitrary precision possible [45]. Such calculations lead to a significantly larger saturation value for $N = 800$ (using 10 000 samples for each point in time and averaging over several times of order $\ln\ln t \sim 4$). However, while the saturation value for $N = 1600$ also increases, we still find eigenvalues in many samples which are effectively zero even in double-double precision. Here quadruple precision would be required to obtain the saturation value reliably. Unfortunately, the computational costs for such calculations are becoming prohibitive. The data for the saturation values which are reliable in double-double precision can be fitted by a logarithm (see inset of Fig. 11). However, given the limited range of accessible system sizes, this fit is not fully convincing. We also note that the ratio of the prefactor of the $\ln\ln t$ scaling and the possible $\ln \ell$ scaling is $a/b = 1.5$ instead of 2 as expected from Eqs. (18) and (19).

Another possible issue is that Eq. (19) applies to a block in an infinite system, while the block in our calculations is exactly half of the system. In Fig. 12 we therefore present, in addition, results where we investigate the scaling of the saturation value more systematically as a function of block size ℓ.

Again, we expect that small blocks are not in the scaling regime and that the data for $N > 400$ become unreliable due

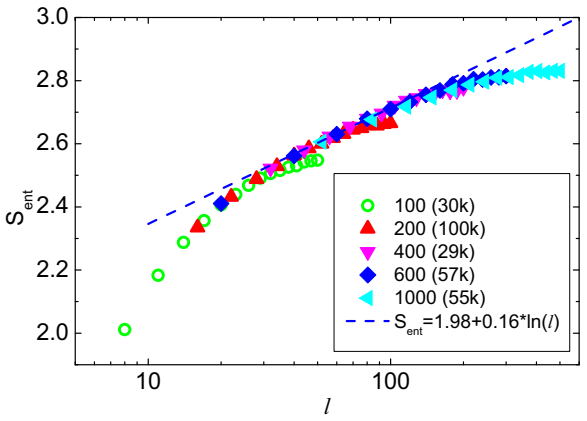

FIG. 12. Double-precision results: Saturation value $S_{\rm ent}(\ell, t \to \infty)$ for a quench from the initial state (3) in the periodic XX chain with $J_i \in (0,1)$ and various chain lengths N and block sizes ℓ as indicated. The dashed line is a fit representing potential logarithmic scaling.

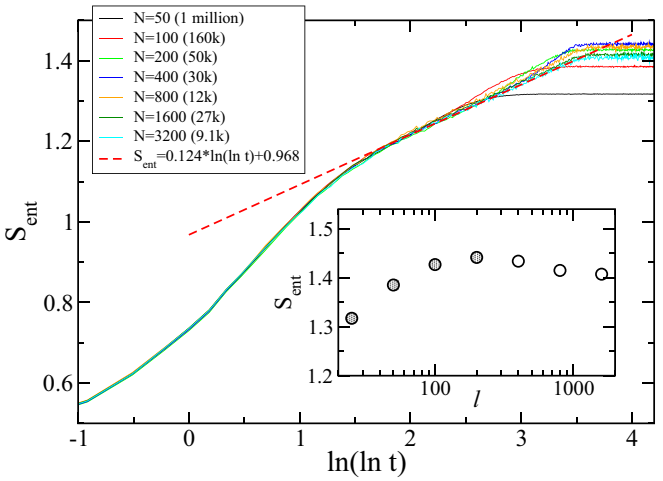

FIG. 13. Same as Fig. 11, but with open instead of periodic boundary conditions. The $N = 3200$ data are fitted, and a $\ln(\ln t)$ scaling is observed. Inset: Saturation value as a function of block length $\ell = N/2$.

to the limited numerical precision. Nevertheless, deviations from a logarithmic scaling (indicated by the dashed line in Fig. 12) appear to be also present for block sizes $\ell \sim 100$–200 and $N \leqslant 400$, where we expect to be in the scaling regime and expect the numerical data to be reliable. In conclusion, our numerical data are insufficient to show unambiguously whether or not the logarithmic scaling, Eq. (19), holds. Note that a saturation $\lim_{\ell\to\infty} \lim_{t\to\infty} S_{\rm ent}(\ell, t) = \text{const}$ would also imply that $S_{\rm ent} \sim \ln\ln t$ is just a transient and not the true scaling behavior.

We find an even more intricate behavior when analyzing the numerical data for the same set of parameters as in Fig. 11 but with open instead of periodic boundary conditions. The results of calculations in double precision are shown in Fig. 13.

The entanglement entropy $S_{\rm ent}(t)$ at late times is now a nonmonotonic function of block size $\ell = N/2$; in particular, the saturation value $S_{\rm ent}(\ell)$ appears to have a maximum at $\ell = N/2 \approx 200$ and to approach a finite value for $\ell \to \infty$ from above (see inset of Fig. 13). Note, however, that the data for $\ell = N/2 > 200$ at long times are again affected by problems with the numerical precision. Nevertheless, the data for $N = 50$–200 are all in the scaling regime and appear reliable, yet a clear logarithmic scaling is not observed. The nonmonotonic behavior in time is apparently a consequence of the interplay of finite block size and boundary contributions. In the regime where $S_{\rm ent} \sim \ln(\ln t)$ we find to a very good accuracy that $S_{\rm ent}^{\rm PBC}(t) = 2S_{\rm ent}^{\rm OBC}(t)$ (see the fits in Figs. 11 and 13). For large system sizes the two cuts between the system block of length ℓ and the environment of length $N - \ell$ in the case of periodic boundary conditions therefore each give a contribution equivalent to the single cut for open boundaries.

The RSRG-X predictions, Eqs. (18)–(20), and our numerical analysis so far are for a quench starting from the density-wave state (3). This is a special state, and the observed growth of the entanglement entropy might therefore not be generic [38,46]. To investigate this point we show in Fig. 14 additional data sets where we quench from a random initial product state.

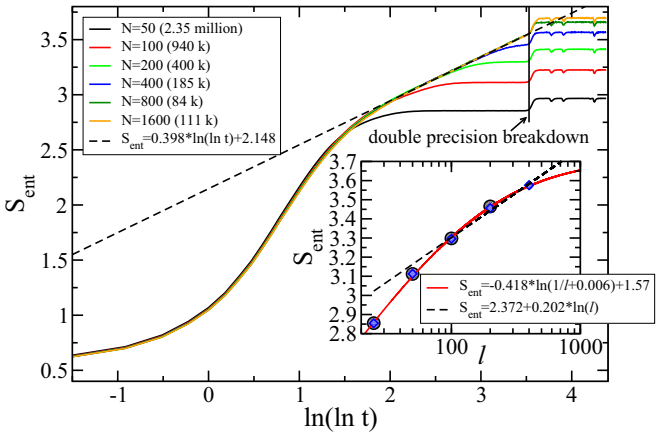

FIG. 14. Same as Fig. 11, but with quenching from a random initial product state instead of the density-wave state (3). Inset: Saturation value, with circles denoting results in double precision and diamonds denoting results in double-double precision.

We do again find a very clear $\ln(\ln t)$ scaling in a certain time window; however, the prefactor is quite different from the one found for the quench from the density wave state. At $\ln(\ln t) \approx 3.5$ the double-precision calculations break down, leading to an artificial jump in $S_{\rm ent}(t)$. We can therefore only extract the saturation values for $\ell = N/2 \leqslant 200$ in double precision and for $\ell = N/2 \leqslant 400$ in double-double precision (see the inset of Fig. 14). The saturation values could be consistent either with a $\ln \ell$ scaling or with a saturation $S_{\rm ent} \approx 3.7$ for $\ell \to \infty$. Assuming that a logarithmic scaling does hold, the fits in Fig. 14 yield a ratio $a/b = 1.97$, which is close to 2 as expected based on the RSRG analysis.

Finally, we analyze the short-time behavior of $S_{\rm ent}(t)$ for periodic-boundary-condition quenching from the density-wave state (see Fig. 15).

We find that the initial increase can be fitted by the function displayed in Fig. 15 and appears almost logarithmic when viewed in a limited time interval. This should be kept in mind when analyzing numerical data for small interacting systems where a logarithmic increase of the entanglement entropy is usually understood as a signature of a many-body localized phase [16]. The data in Fig. 15 show that a very similar behavior in a restricted time window can also be observed in a critical disordered noninteracting system. This is consistent with previous findings by Chiara *et al.* [40].

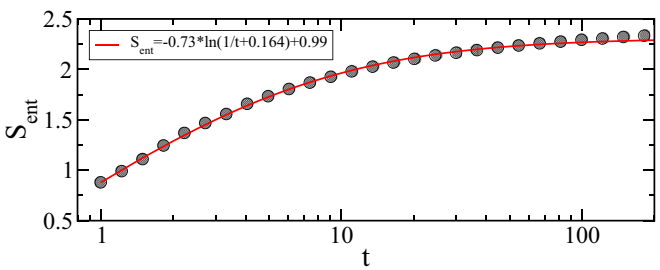

FIG. 15. $S_{\rm ent}(t)$ for the XX model with bond disorder $J_i \in (0,1)$, PBC, and quenching from the density-wave state. The line is a fit, showing that the initial increase is almost logarithmic in time.

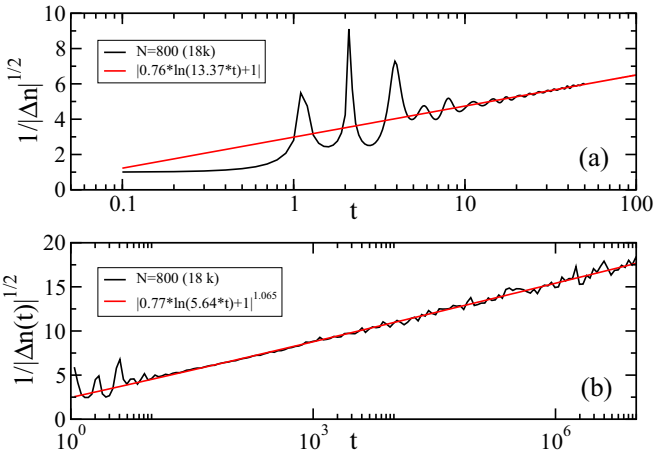

FIG. 16. Decay of $\Delta n(t)$, Eq. (10), in the XX model with bond disorder $J_i \in [0,1)$, $N = 800$ sites, PBC, and averaging over 18 000 samples. (a) Short-time behavior and (b) long-time decay.

As for the potential disorder case, we also consider the decay of the density-wave order parameter (10) in a quench from the initial state (3) for bond disorder.

In Fig. 16 we plot $1/\sqrt{|\Delta n|}$ as a function of time. The fit in Fig. 16(a) for times $t \in [20,50]$ shows that the decay is consistent with the RSRG-X prediction, Eq. (20). Here we have kept the exponent fixed. In Fig. 16(b) a similar fit with $t \in [20,10^6]$ is presented, where the exponent is also used as a fitting parameter. The result is consistent with the fit at short times. Note that Eq. (20) is, strictly speaking, only valid in an infinite system. For any finite system and any given disorder configuration we will ultimately expect recurrences. Due to the disorder average and the broad distribution of couplings J_i, however, the asymptotic decay of the order parameter can be observed over several orders of magnitude in time in a system with only $N = 800$ sites.

B. Binary distribution

Instead of bond disorder drawn from a box distribution as investigated in the previous section, we will consider here binary bond disorder $J_i = 1 \pm \delta$. This case is interesting not only because it allows for a numerical investigation of infinite chains even if interactions are added (see Sec. V) but also because the applicability of the RSRG-X approach seems questionable in this case. In the RSRG-X, fast dynamics caused by the strongest bonds in the random chain is eliminated, and the couplings between the remaining degrees of freedom are renormalized. The control parameter is the ratio of the coupling constants to the two adjacent sites over the coupling of the strong bond. For binary disorder, where the chain consists of segments with length $\ell = 2,3,\ldots$ with the *same* coupling $J = 1+\delta$ or $J = 1-\delta$, this ratio will often be equal to 1. Instead, one might therefore start by eliminating segments of strong bonds beginning with the shortest ones, which are responsible for the fastest dynamics. This will lead to a broader distribution of couplings for which a standard RSRG approach might again be applicable. However, long segments with strong couplings $J = 1+\delta$ will show an internal slow dynamics not captured in

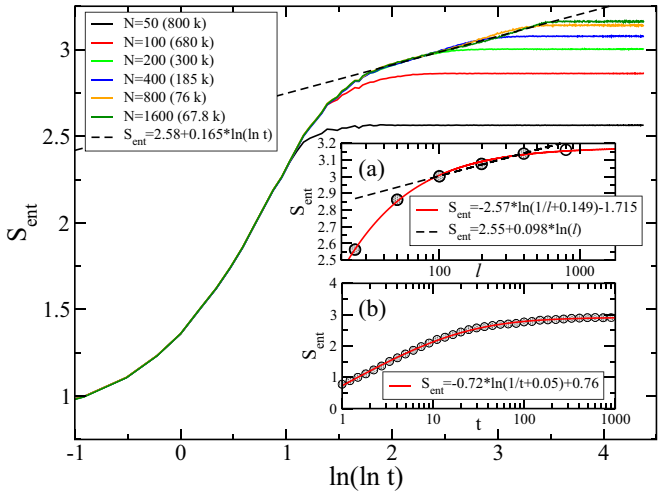

FIG. 17. $S_{\rm ent}(t)$ for the XX model with binary bond disorder $\delta = 0.4$ and OBC. Fit of the $N = 1600$ data (dashed line). Inset (a) shows saturation value $S_{\rm ent}(\ell, t \to \infty)$, and inset (b) shows approximately logarithmic scaling of $S_{\rm ent}(t)$ for $t \leqslant 1000$.

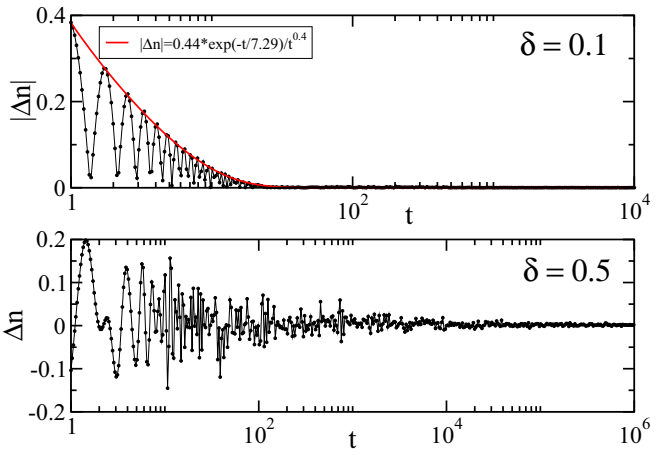

FIG. 18. $\Delta n(t)$ for the XX model with $N = 800$ sites, 40 000 samples, and binary bond disorder δ as indicated. The lines are a guide to the eye.

such an approach, so that it is *a priori* unclear if such a modified RSRG-X description can become correct asymptotically.

In Fig. 17 data for a quench with the initial state (3), OBC, and $\delta = 0.4$ are shown. Qualitatively, the results are surprisingly similar to the case of a box distribution. The initial increase of $S_{\rm ent}(t)$ is again approximately logarithmic up to times $t \approx 10^3$ [see Fig. 17, inset (b)]. For $t \in [10^4, 10^{14}]$ and $N = 1600$ we find a scaling regime with $S_{\rm ent}(t) \sim 0.165 \ln(\ln t) + 2.58$. While this is qualitatively the same behavior as for the box distribution, the prefactor is different when compared to the fit in Fig. 13 (0.165 as compared to 0.124). The saturation values are reached quicker than for the box distribution, and data up to $\ell = N/2 = 400$ should be reliable in double precision. All the data can be fitted by the function shown as a solid line in inset (a) of Fig. 17, leading to a finite saturation value, $\lim_{\ell\to\infty} S_{\rm ent}(\ell, t \to \infty) \approx 3.18$, in the thermodynamic limit. However, the data for $N = 50, 100$ are not in the scaling regime. Excluding these data, a logarithmic fit is also possible; see the dashed line in inset (a) in Fig. 17. Again, we cannot unambiguously show numerically whether or not Eq. (19) holds.

Also interesting is the time evolution of the density-wave order parameter, Eq. (10). For $\delta = 1$ the chain separates into finite segments, and $\Delta n(t)$ oscillates around $\overline{\Delta n} = 1/3$ exactly as for the case of infinite binary potential disorder (see Fig. 9). The only difference is that time is now rescaled by a factor 2 because the hopping along the chain segments is given by $J = 1 + \delta = 2$ instead of $J = 1$ for the case of infinite binary potential disorder. For $0 < \delta < 1$ we expect $\Delta n(t)$ to decay for long times in an infinite chain. Note, however, that the weak bonds introduce a dephasing time scale $t_p = 1/(1 - \delta)$ which diverges for $\delta \to 1$. In our numerical analysis we therefore concentrate on small and intermediate strengths of binary disorder. Results for $\Delta n(t)$ with $\delta = 0.1$ and $\delta = 0.5$ are shown in Fig. 18.

For $\delta = 0.1$ the density-wave order decays quickly, and the envelope can be very well fitted by an exponential with an algebraic correction. For $\delta = 0.5$ the density-wave order parameter also decays; however, the strong oscillations make it difficult to observe any clear scaling. In both cases, the asymptotics (20) predicted by RSRG-X is not observed. Note, however, that it is very difficult to analyze the regime of long times where $|\Delta n|$ is small and the relative fluctuations are large, so that it is impossible to draw any definite conclusions from the numerical data.

IV. CRITICAL RANDOM TRANSVERSE ISING MODEL

As a second example for a critical random model, we consider the transverse Ising model

$$H = -\sum_{i=1}^{N} \left\{ J_i \sigma_i^x \sigma_{i+1}^x + h_i \sigma_i^z \right\} \tag{21}$$

with periodic boundary conditions. This model can be mapped onto a chain of free fermions of length $2N$ [15,47–49]. The entanglement entropy can therefore be calculated using the same single-particle algorithms as used previously for the XX model. If J_i and h_i are drawn independently of the same distribution function, then the model (21) is critical; otherwise, we are in an ordered or disordered phase.

The DOS and the localization measure (9) already give clear indications of critical behavior. As shown in Fig. 19(a), the density of states diverges in the critical case for $|\varepsilon| \to 0$ in the thermodynamic limit. The divergence is consistent with the analytically obtained formula (15) for the XX model. At the same time, the localization measure I_ε as defined in Eq. (9) goes to zero for $\varepsilon \to 0$, indicating a delocalization transition at zero energy [see Fig. 19(b)].

The time evolution of the entanglement entropy in the random transverse Ising model following a global quench was studied first by Iglói *et al.* [15]. For the critical case they found a regime where $S_{\rm ent}(t) \approx 0.25 \ln(\ln t) + \text{const}$. Furthermore, their data seem to indicate that $S_{\rm ent}(\ell, t \to \infty) \approx 0.173 \ln \ell + \text{const}$. This scaling would be qualitatively consistent with the RSRG-X predictions, Eqs. (18) and (19), although the values of the prefactors as well as their ratio are different. On the other hand, we have not found fully conclusive evidence for a $\ln \ell$ scaling of the saturation value for the XX model. To

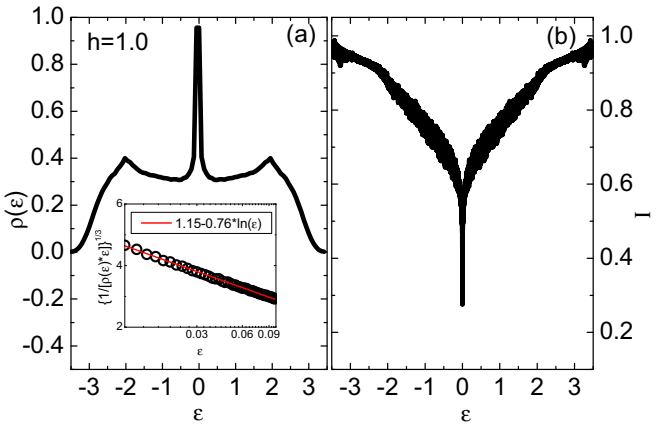

FIG. 19. Critical random transverse Ising model with $J_i \in (0,1)$ and $h_i \in (0,1)$: (a) DOS as defined in Eq. (8) using 10 000 samples with 100 bins (main) and 3400 bins (inset). (b) Localization measure (9) with $m = 10$.

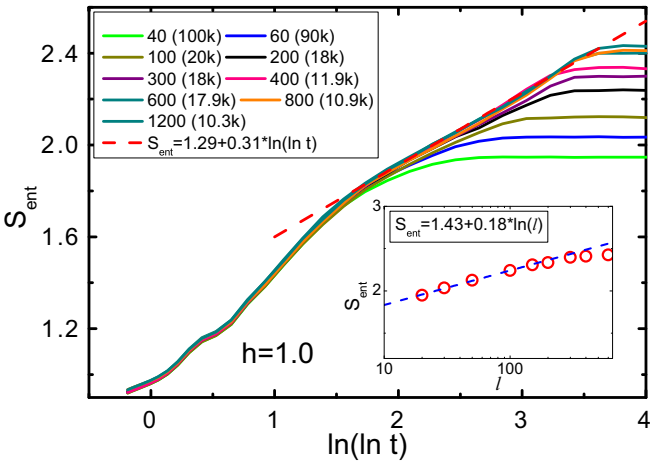

FIG. 20. $S_{\rm ent}(t)$ in the random critical transverse Ising model with PBC for a quench from the initial state (3) with block size $\ell = N/2$. Inset: Saturation value $S_{\rm ent}(\ell, t \to \infty)$.

resolve this discrepancy we will, in the following, extend the calculations in Ref. [15] to larger system sizes. Numerically, this is a demanding task. For system sizes larger than $N = 300$ we again encounter samples with very small eigenvalues where the regular double-precision diagonalization routine fails to return a set of fully converged eigenvalues and eigenvectors. Here the problem is even more severe because the linear dimension of the Hamiltonian matrix is a factor of 2 larger ($2N \times 2N$ for the Ising model instead of $N \times N$ for the XX model). A straightforward but very time-consuming way to deal with this problem is to diagonalize such problematic samples using multiprecision routines. This is the way we have chosen to address this problem for the XX model. Here we use a different approach where samples with extremely small eigenvalues and a not fully converged spectrum are simply discarded. This approach should not affect the data for times $t < 10^{14}$ but makes the results for larger times unreliable. A further confirmation that this is a valid approach is that the entanglement curves for various system sizes fall on top of each other if $t < 10^{14}$ and if the entanglement length $L(t)$ is smaller than the block length ℓ (see Fig. 20).

The entanglement entropy shows qualitatively the same behavior as for the XX model with bond disorder and PBC. In particular, we find a regime of $\ln(\ln t)$ scaling. The slope is comparable to the one we found for the XX model with the bond couplings drawn from a box distribution and overall is consistent with previous results by Iglói *et al.* [15]. Our main new result concerns the saturation value $S_{\rm ent}(\ell, t \to \infty)$ shown in the inset of Fig. 20: Here we obtain data which, we believe, are reliable at least up to $\ell = N/2 = 200$. In agreement with Ref. [15], in which systems up to the maximum system size $N = 256$ were studied, we find that the saturation values are consistent with a $S_{\rm ent} \sim \ln \ell$ scaling. The saturation for chain lengths $N > 400$, on the other hand, occurs at times $t > 10^{14}$ and might already be affected by the discarding of samples with extremely small eigenvalues. The ratio of the prefactors of the $\ln \ln t$ and the $\ln \ell$ fits is $a/b = 1.7$ in this case.

To investigate the scaling of the saturation value in more detail we show data for different chain lengths N and different block sizes ℓ in Fig. 21.

These data cast some doubt on whether a $\ln \ell$ scaling really holds. Deciding this question would require computationally very expensive multiprecision calculations. As for the XX model, we have to leave this as an open problem for future investigations.

V. INTERACTING MODELS

We will concentrate on the XXZ chain with binary bond disorder

$$H = \sum_i J_i \{(c_i^\dagger c_{i+1} + \text{H.c.}) + \Delta(n_i - 1/2)(n_{i+1} - 1/2)\} \tag{22}$$

and nearest-neighbor interaction $\Delta > 0$. Here $J_i = 1 \pm \delta$, $n_i = c_i^\dagger c_i$ is the local-density operator, and we are using the fermionic representation of the XXZ model. The clean system,

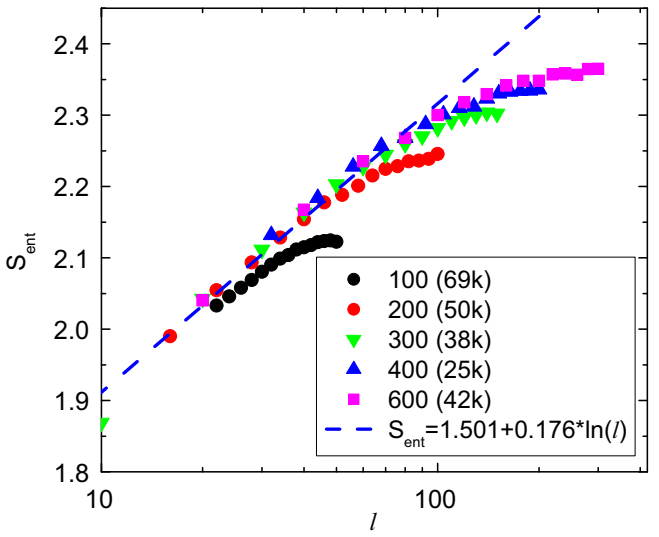

FIG. 21. Saturation value $S_{\rm ent}(\ell, t \to \infty)$ for a quench from the initial state (3) in the critical transverse Ising chain for various chain lengths N as indicated. The dashed line is a fit representing potential logarithmic scaling.

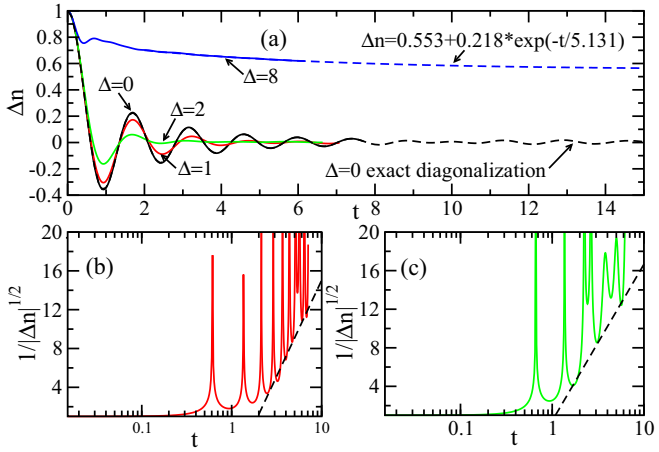

FIG. 22. (a) $\Delta n(t)$ for binary disorder $\delta = 0.2$ and different interaction strengths Δ obtained by LCRG for an infinite chain. The dashed line for $\Delta = 0$ is the exact diagonalization result; the dashed line for $\Delta = 8$ is a fit. (b) $\Delta n(t)$ for $\Delta = 1$ (solid line) and a fit of the envelope (dashed line). (c) Same as in (b), but for $\Delta = 2$.

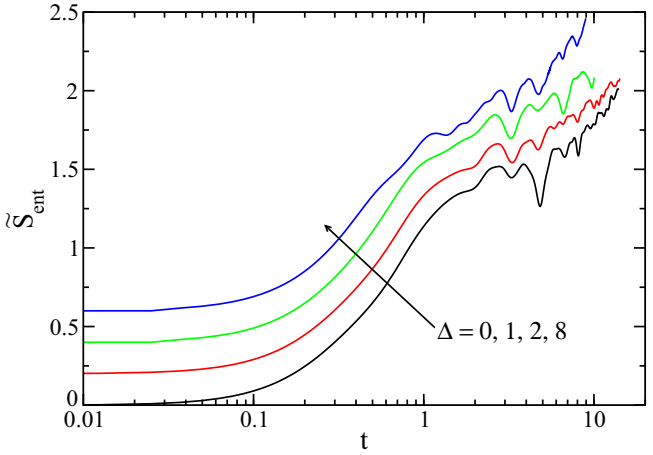

FIG. 23. LCRG data for $\tilde{S}_{\rm ent}(t)$ of a system consisting of real sites and ancilla sites which realize binary bond disorder with $\delta = 0.92$ exactly. Subsequent curves are shifted by 0.2.

$J_i \equiv J$, is critical for $-2 \leqslant \Delta \leqslant 2$ and is gapped otherwise. The model (22) has been investigated by RSRG-X for the specific case of a quench from the density-wave state (3) in Ref. [38] and by exact diagonalizations, concentrating mainly on spectral properties, in Ref. [46].

Calculating the quench dynamics now becomes a true many-body problem, and the methods we have used before are no longer applicable. Instead, we use exact diagonalizations of the many-body Hamiltonian for small system sizes as well as the light-cone renormalization group (LCRG) [9,17], a variant of the DMRG, to treat infinite XXZ chains. First, we consider the time evolution of the order parameter $\Delta n(t)$. For the case without disorder, numerical studies have found that the scaling of Δn at short and intermediate times seems consistent with an exponential decay [9,50,51]. Here we want to study how this decay is affected by disorder. In Fig. 22 we present data for binary disorder $\delta = 0.2$ and different interaction strengths Δ.

For $\Delta = 1$ and $\Delta = 2$ the data indicate that $\Delta n(t) \to 0$ for $t \to \infty$. As shown in Figs. 22(b) and 22(c), respectively, the decay could possibly be consistent with Eq. (20). Note, however, that in the noninteracting case where data for much larger times are available (see Fig. 18) a clear scaling over several orders of magnitude in time is not observed. What is clear, however, is that the decay for $\Delta = 1$ and $\Delta = 2$ does not follow a simple exponential as in the clean case, suggesting that the system is no longer in the same ergodic phase. This becomes even more apparent for $\Delta = 8$, where the density-wave order becomes effectively frozen and a fit of the data seems consistent with $\Delta n \neq 0$ at infinite times.

Next, we consider the entanglement entropy in the interacting case. In the LCRG algorithm the binary bond disorder is realized by ancilla sites which are prepared in a completely mixed state. A partial trace then yields the reduced density matrix of real *and* ancilla sites [17]. The ancilla sites, however, are static, so that the entanglement entropy $\tilde{S}_{\rm ent}(t)$ of the system with real and ancilla sites will show the same scaling behavior as the entanglement entropy $S_{\rm ent}(t)$ of the system with only real sites. The absolute values of the two entropies will, however, be different. In Fig. 23, $\tilde{S}_{\rm ent}$ is shown for strong binary disorder $\delta = 0.92$ and different interaction strengths.

After an initial increase, we find a regime where the entanglement entropy seems to scale approximately logarithmically for all interaction strengths, including the noninteracting case and the isotropic case $\Delta = 2$. Theoretically, however, these cases are expected to show quite different behaviors. For the quench from the density-wave state and with $|\Delta| < 2$, RSRG-X predicts $S_{\rm ent} \sim (\ln t)^{2/\phi}$, with $\phi = (1 + \sqrt{5})/2$ being the golden ratio. For the isotropic case arguments based on results for $SU(2)_k$ chains suggest that in the Heisenberg limit ($k \to \infty$) the system becomes ergodic and shows volume-law entanglement scaling [52]. For the time interval shown, such differences are not observed. While LCRG data for longer times can, in principle, be obtained, the calculations require a substantial amount of computing time, and it is unclear if a factor of 2–3 in time would be sufficient to change this picture.

Next, we turn to the exact diagonalization of small systems where long times are accessible. We concentrate on the case $\Delta = 2$, which corresponds to the isotropic Heisenberg model if the Hamiltonian (22) is formulated in terms of spin-1/2 operators. In this case we can make use of the SU(2) symmetry, which allows us to diagonalize larger systems than in the anisotropic case where SU(2) is broken. In Fig. 24 data for several system sizes are shown.

For $N \geqslant 12$, a logarithmic scaling seems to emerge at times which are much larger than the simulation times in the LCRG calculations. This is very different from our previous study of binary potential disorder [17], where we could clearly distinguish the Anderson insulator from the many-body localized system for times accessible by LCRG. The results seem to indicate that there exists a many-body localized phase for the bond-disordered Heisenberg model. However, we cannot exclude that longer chains show a different scaling consistent with thermalization, as predicted in Ref. [52].

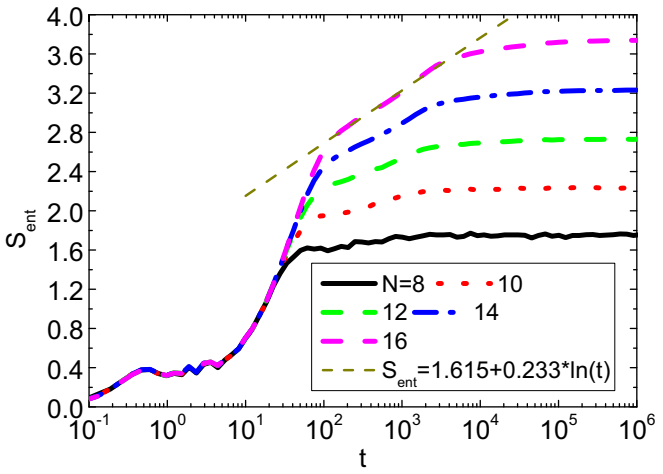

FIG. 24. Exact diagonalization data for the isotropic XXZ model ($\Delta = 2.0$) with binary bond disorder $\delta = 0.92$. Averages are performed over 15 000 samples for $L < 16$ and 11 600 samples for $L = 16$.

VI. CONCLUSIONS

We have numerically analyzed the entanglement growth in disordered noninteracting and interacting quantum chains following a quantum quench. While most papers so far have concentrated on the case of potential disorder, our study has focused on bond disordered models. The latter systems are highly relevant theoretically because the real-space renormalization group can be applied in this case, allowing for a direct comparison between renormalization-group predictions and numerical data.

As a first step, we compared the localization of the single-particle wave functions in the XX model in the potential-disordered case with the bond-disordered case. While potential disorder leads to a localization length $\xi_{\rm loc}$ which only weakly depends on the energy ε of the wave function, a delocalization transition, where the localization length diverges, occurs at $\varepsilon = 0$ for bond disorder. This has profound consequences for the buildup of entanglement: $S_{\rm ent}(t)$ for the potential-disordered case shows an initial power-law increase followed by saturation. The $S_{\rm ent}(t)$ curve becomes independent of system size N and block size ℓ for $N, \ell \gg \xi_{\rm loc}$. For bond disorder, on the other hand, the behavior is much more complex. An initial approximately logarithmic increase, $S_{\rm ent} \propto -\ln(1/t + \alpha)$ with $\alpha \ll 1$, is followed by a $S_{\rm ent} \sim \ln\ln t$ scaling over several orders of magnitude in time and a saturation which depends on the block size.

The main focus of our work was on a comparison of the numerical results for $S_{\rm ent}(t)$ and for the density-wave order parameter $\Delta n(t)$ with predictions by the RSRG. For the XX model there are three main predictions for a block of size ℓ in an infinite system following a quench from a density wave state: (i) In the scaling regime at long times $S_{\rm ent} \sim a \ln\ln t$, (ii) the saturation value scales as $S_{\rm ent} \sim b \ln \ell$, and (iii) the order parameter decays as $\Delta n \sim 1/\ln^2 t$. Numerically, we find the decay of the order parameter to be consistent with the RSRG result. The analysis of the entanglement entropy, on the other hand, turns out to be much more complicated. Here extremely long times are necessary to study saturation as a function of block size ℓ. In order to reach such times we performed very time-consuming multiprecision calculations, which are needed because the spectrum of bond disordered chains contains many extremely small eigenvalues. Even with such data at hand, an unbiased numerical confirmation of the RSRG predictions for the entanglement entropy turned out to be out of reach. The main question which we have to leave open is as to whether the saturation value scales as $S_{\rm ent} \sim b \ln \ell$ as predicted by RSRG or saturates in the limit of infinite block size, $S_{\rm ent} \sim -\ln(1/\ell + \alpha)$, where $0 < \alpha \ll 1$ is a constant. For the time dependence of the entanglement entropy this means that we cannot decide if $S_{\rm ent} \sim a \ln\ln t$ is just a transient behavior valid in a certain time range or if it does indeed hold for all times in the limit $\ell \to \infty$. Furthermore, we find that even if we take a $\ln \ell$ scaling as a given, a best fit yields a ratio $a/b \approx 1.5$, which significantly deviates from $a/b = 2$ expected based on the RSRG analysis.

The RSRG scaling predictions should also be valid for the critical random transverse Ising chain. This model can be mapped to free fermions, so that a numerical study based on single-particle wave functions is possible. Our results for the entanglement entropy in this case are qualitatively in agreement with the results for the XX model. We again find $S_{\rm ent} \sim a \ln\ln t$ in a certain time range but cannot obtain reliable data for large enough systems and long enough times to decide whether or not the predicted $S_{\rm ent} \sim b \ln \ell$ scaling of the saturation value holds. Assuming that the scaling holds, we find from a best fit that $a/b \approx 1.7$, which again deviates from the RSRG result.

Finally, we studied the interacting XXZ model with binary bond disorder. Using an infinite-size density-matrix renormalization-group algorithm, we found that the entanglement entropy shows a $S_{\rm ent} \sim \ln t$ scaling both in the interacting case and in the free-fermion case $\Delta = 0$. In the accessible time range it is thus not possible to distinguish an Anderson insulator from a system which is expected to be in a (critical) many-body localized phase. The exact diagonalization of small interacting systems with large binary potential disorder shows that the true scaling regime is only reached at times which are much larger than the simulation times in the density-matrix renormalization-group calculations. The exact diagonalizations also seem to provide indications that the Heisenberg model at strong binary bond disorder is in a many-body localized phase. However, due to the limited system sizes which are accessible numerically, the theoretically predicted ergodicity of the bond-disordered Heisenberg model, based on results for $SU(2)_k$ chains, cannot be excluded.

ACKNOWLEDGMENTS

We acknowledge support from the Natural Sciences and Engineering Research Council (NSERC, Canada) and are grateful for the computing resources and support provided by Compute Canada and Westgrid. In particular, we would like to thank G. Shamov for his help in installing and using the MPACK libraries.

[1] M. Greiner, O. Mandel, T. Esslinger, T. W. Hänsch, and I. Bloch, Nature (London) **415**, 39 (2002).
[2] I. Bloch, J. Dalibard, and W. Zwerger, Rev. Mod. Phys. **80**, 885 (2008).
[3] S. Ulm, J. Roßnagel, G. Jacob, C. Degünther, S. T. Dawkins, U. G. Poschinger, R. Nigmatullin, A. Retzker, M. B. Plenio, F. Schmidt-Kaler *et al.*, Nat. Commun. **4**, 2290 (2013).
[4] G. Vidal, Phys. Rev. Lett. **91**, 147902 (2003).
[5] G. Vidal, Phys. Rev. Lett. **93**, 040502 (2004).
[6] A. J. Daley, C. Kollath, U. Schollwöck, and G. Vidal, J. Stat. Mech. (2004) P04005.
[7] S. R. White and A. E. Feiguin, Phys. Rev. Lett. **93**, 076401 (2004).
[8] J. Sirker and A. Klümper, Phys. Rev. B **71**, 241101(R) (2005).
[9] T. Enss and J. Sirker, New J. Phys. **14**, 023008 (2012).
[10] U. Schollwöck, Ann. Phys. (N.Y.) **326**, 96 (2011).
[11] P. Calabrese and J. Cardy, Phys. Rev. Lett. **96**, 136801 (2006).
[12] P. Calabrese and J. Cardy, J. Stat. Mech. (2005) P04010.
[13] N. Laflorencie, arXiv:1512.03388.
[14] M. Žnidarič, T. Prosen, and P. Prelovšek, Phys. Rev. B **77**, 064426 (2008).
[15] F. Iglói, Z. Szatmári, and Y.-C. Lin, Phys. Rev. B **85**, 094417 (2012).
[16] J. H. Bardarson, F. Pollmann, and J. E. Moore, Phys. Rev. Lett. **109**, 017202 (2012).
[17] F. Andraschko, T. Enss, and J. Sirker, Phys. Rev. Lett. **113**, 217201 (2014).
[18] C. Holzhey, F. Larsen, and F. Wilczek, Nucl. Phys. B **424**, 443 (1994).
[19] P. Calabrese and J. Cardy, J. Phys. A **42**, 504005 (2009).
[20] E. H. Lieb and D. W. Robinson, Commun. Math. Phys. **28**, 251 (1972).
[21] S. Bravyi, M. B. Hastings, and F. Verstraete, Phys. Rev. Lett. **97**, 050401 (2006).
[22] M.-C. Chung and I. Peschel, Phys. Rev. B **64**, 064412 (2001).
[23] I. Peschel, J. Stat. Mech. (2004) P06004.
[24] I. Peschel and V. Eisler, J. Phys. A **42**, 504003 (2009).
[25] D. M. Basko, I. L. Aleiner, and B. L. Altshuler, Ann. Phys. (N.Y.) **321**, 1126 (2006).
[26] R. Nandkishore and D. A. Huse, Annu. Rev. Condens. Matter Phys. **6**, 15 (2015).
[27] E. Altman and R. Vosk, Annu. Rev. Condens. Matter Phys. **6**, 383 (2015).
[28] A. Pal and D. A. Huse, Phys. Rev. B **82**, 174411 (2010).
[29] E. Abrahams, P. W. Anderson, D. C. Licciardello, and T. V. Ramakrishnan, Phys. Rev. Lett. **42**, 673 (1979).
[30] T. P. Eggarter and R. Riedinger, Phys. Rev. B **18**, 569 (1978).
[31] D. S. Fisher, Phys. Rev. B **50**, 3799 (1994).
[32] D. S. Fisher, Phys. Rev. Lett. **69**, 534 (1992).
[33] D. S. Fisher, Phys. Rev. B **51**, 6411 (1995).
[34] L. Balents and M. P. A. Fisher, Phys. Rev. B **56**, 12970 (1997).
[35] G. Refael and J. E. Moore, Phys. Rev. Lett. **93**, 260602 (2004).
[36] N. Laflorencie, Phys. Rev. B **72**, 140408 (2005).
[37] D. Pekker, G. Refael, E. Altman, E. Demler, and V. Oganesyan, Phys. Rev. X **4**, 011052 (2014).
[38] R. Vosk and E. Altman, Phys. Rev. Lett. **110**, 067204 (2013).
[39] R. Vosk and E. Altman, Phys. Rev. Lett. **112**, 217204 (2014).
[40] G. D. Chiara, S. Montangero, P. Calabrese, and R. Fazio, J. Stat. Mech. (2006) P03001.
[41] M. Schreiber, S. S. Hodgman, P. Bordia, H. P. Lüschen, M. H. Fischer, R. Vosk, E. Altman, U. Schneider, and I. Bloch, Science **349**, 842 (2015).
[42] D. Pertot, A. Sheikhan, E. Cocchi, L. A. Miller, J. E. Bohn, M. Koschorreck, M. Köhl, and C. Kollath, Phys. Rev. Lett. **113**, 170403 (2014).
[43] R. C. Brown, R. Wyllie, S. B. Koller, E. A. Goldschmidt, M. Foss-Feig, and J. V. Porto, Science **348**, 540 (2015).
[44] B. Paredes, F. Verstraete, and J. I. Cirac, Phys. Rev. Lett. **95**, 140501 (2005).
[45] M. Nakata, MPACK, http://mplapack.sourceforge.net.
[46] R. Vasseur, A. J. Friedman, S. A. Parameswaran, and A. C. Potter, Phys. Rev. B **93**, 134207 (2016).
[47] P. Pfeuty, Phys. Lett. A **72**, 245 (1979).
[48] E. Lieb, T. Schultz, and D. Mattis, Ann. Phys. (N.Y.) **16**, 407 (1961).
[49] F. Iglói, Z. Szatmári, and Y.-C. Lin, Phys. Rev. B **80**, 024405 (2009).
[50] P. Barmettler, M. Punk, V. Gritsev, E. Demler, and E. Altman, Phys. Rev. Lett. **102**, 130603 (2009).
[51] P. Barmettler, M. Punk, V. Gritsev, E. Demler, and E. Altman, New J. Phys. **12**, 055017 (2010).
[52] R. Vasseur, A. C. Potter, and S. A. Parameswaran, Phys. Rev. Lett. **114**, 217201 (2015).